# A PRE-STACK DEPTH DIFFRACTION IMAGING WORKFLOW BASED ON ANGLE GATHERS

JIANGJIE ZHANG

*Institute of Geology and Geophysics, Chinese Academy of Sciences, Beijing 100029, P.R. China.*

(Received April 26, 2012; revised version accepted February 15, 2013)

ABSTRACT

Zhang, J., 2013. A pre-stack depth diffraction imaging workflow based on angle gathers. *Journal of Seismic Exploration*, 22: 129-145.

A new workflow is presented that can image diffracted waves for pre-stack seismic data based on angle gathers. This workflow combines the advantages of pre-stack time migration and pre-stack depth migration. For simplicity in calculations and parameter estimations, we mute the Fresnel zones related to reflections to enhance diffractions in the common angle gathers by shot-domain pre-stack time migration. A structural dip estimation scheme is provided to obtain the best Fresnel zones for accurate attenuation of reflections. Then, the demigration processing is used to remove the effect of previous pre-stack time migration on the imaged diffracted events to obtain diffracted wavefield. At last, the diffracted wavefield is imaged again by pre-stack depth migration, which adapt to imaging for complex structure. The result of my method is an effective complement to conventional interpretation workflow in detecting of small-scale geological discontinuities. Synthetic example and field data example demonstrate that my method is accurate, robust and easy to implement.

KEY WORDS: diffraction imaging, Fresnel zone, angle gather, structural dip, demigration.

## INTRODUCTION

Seismic diffracted waves are response of small scale geological discontinuities such as faults, pinch-outs and fractures. Correct identification and use of diffracted wave are important for interpretation, velocity estimation (Reshef and Landa, 2009; Sava et al., 2004) or detecting and mapping fracture corridors (Chen and Hilterman, 2007). Also, any successful attempt at resolving structural details on a sub-wavelength scale (super-resolution) is most likely to

0963-0651/13/$5.00 

rely on diffractions (Bertero et al., 1996). Throughout the years, diffracted waves have been under attention of several authors. Kovalevsky (1971) noted and experimentally confirmed the existence of seismic anomalies associated with small-amplitude faults in the subsurface. Landa and Maksimov (1980) demonstrated the possibility of identifying diffraction events in seismic data and using them for detection of small scale structural elements.

The main challenge in the application of diffracted wave is that the amplitudes of diffractions are typically one or two orders of magnitude weaker than the amplitudes of reflections. Thus, most diffraction essentially is lost during the conventional stack or migration processing. Efficient separation between reflected and diffracted wavefields and subsequent imaging of the diffracted component are helpful in retrieving the diffraction information. Bansal and Imhof (2005) proposed a data processing workflow to enhance diffracted component while suppressing reflected events. They discussed the advantages and limitations of several methods, in which NMO and dip filtering were applied to remove flattened reflected events. Khaidukov et al. (2004) proposed a focusing-defocusing approach based on focusing reflected waves to their imaginary source points and then muting them from the full wavefield. Moser and Howard (2008) designed an additional weighting function to the migration kernel that is used to suppress specular reflections in order to image the diffracted waves. The key problem of these methods is how to choose the thresholds for the separation of diffractions and reflections under non-ideal situations such as complex geological structures.

Another separation method for pre-stack data is described by Taner et al. (2006). They show that plane-wave decomposition naturally separates specular and diffracted events and they use a plane-wave destruction filter to suppress specular events. Goldin et al. (2000) try to separate weak diffractions from strong regular reflections by downward wavefield continuation using Gaussian beams. They proposed an approach to construct selective images which highlight backscatter wave energy at certain angles. There are also other approaches such as combining the separation processing with curvelet-based subtraction (Verschuur et al., 2007), and the local image matrix in pre-stack migration (Zhu and Wu, 2008, 2010). Among all these methods, computation efficiency is the unavoidable problem for practical implementations.

Since the main advantage of pre-stack time migration is the computation efficiency and the estimation of migration and muting parameters, we provide a pre-stack diffraction migration workflow combining the advantages of pre-stack time migration and pre-stack wave equation migration in this paper. We firstly present the formulations to compute the travel-time and amplitude by stationary-phase theory to extract angle gathers by shot-domain pre-stack time migration. Then we evaluate the Fresnel zone of reflection under tilted reflector by the analytical derivation of pre-stack time migration and remove the specular

reflection by muting the Fresnel zone on angle gather. At last, we obtain diffracted wave field from the time-domain diffraction imaging section by demigration and image it by wave equation migration to detect and map the small scale geological discontinuities. Finally, we use numerical and field data example to demonstrate the feasibility of my method.

## METHODOLOGY

The stack of pre-stack time migrated gather is a superposition of dynamic diffraction hyperbolae. Specular reflectors are imaged by constructive interference of the hyperbolae portions belonging to Fresnel zones, while the remainders of hyperbolae are mutually annihilated by destructive interference in the migration processing. On the contrary, weak diffraction events are straight and tangent with reflections in the imaged gather. Since specular reflections are strongly dominating, they can mask diffractions in stacking processing, even if the latter are properly imaged. To make the diffraction better visible, a natural solution is to attenuate the specular reflected components on the imaging hyperbolae.

### Formulations of traveltime and amplitude and extract angle gather

In this section, we first derive the formulations to compute the traveltime and amplitude based on phase-shift theory (Gazdag, 1978; Claerbout, 1985). Assuming a laterally invariant medium, we have the downward continuation of the trace by following the phase-shift method as (Zhang et al., 2012)

$$\tilde{P}(p_x,p_y,\omega,T = \sum_{i=1}^{n} \Delta T_i) = f(\omega)\exp(-j\omega \sum_{i=1}^{n} \Delta T_i \sqrt{\{1 - v_i^2(p_x^2+p_y^2)/\omega^2\}}) \quad , \qquad (1)$$

where n is the number of the vertically invariant layers, j is an imaginary unit, $v_i$ is the velocity within each layer, $\Delta T_i$ is the vertical one-way travel time through each layer, $T = \sum_{i=1}^{n} \Delta T_i$ is the one-way travel time from the shot or geophone to the datum level, $\omega$ is the angular frequency, and $f(\omega)$ is the Fourier transform of source or geophone wavefield. The time-shift in the second term at the right-hand side of eq. (1) can be approximated as

$$\sum_{i=1}^{n} (\Delta T_i \sqrt{\{1 - v_i^2(p_x^2+p_y^2)/\omega^2\}}) \approx \sqrt{\{1 - V_{rms}^2(p_x^2+p_y^2)/\omega^2\}} \cdot (\sum_{i=1}^{n} \Delta T_i) \quad .(2)$$

Using the Taylor expansion and ignore the high order items, we obtain

$$V_{rms}^2 = \sum_{i=1}^{n} v_i^2 \Delta T_i \Big/ \sum_{i=1}^{n} \Delta T_i \quad , \tag{3}$$

where $V_{rms}$ is the well-known root-mean-square velocity used in pre-stack time migration. Substituting eq. (2) into eq. (1), we obtain the F-K domain wave-field by spatial inverse Fourier transform:

$$P(x,y,\omega,T) = (\omega/4\pi^2) \times$$

$$\int \int f(\omega)\exp[-j\omega(\sqrt{\{1 - V_{rms}^2(p_x^2+p_y^2)\}}\cdot T - p_x x - p_y y)]dp_x dp_y \quad . \tag{4}$$

Applying stationary-phase theory (Bleistein, 1984; Docherty, 1991), we have

$$P(x,y,\omega,T)$$

$$= f(\omega)(\omega/2\pi)\exp(-j\pi/2)|Q(p_x^0,p_y^0)|^{-1/2}\exp[-j\omega\phi(p_x^0,p_y^0)] \quad , \tag{5}$$

with

$$\phi(p_x,p_y) = \sqrt{\{1 - V_{rms}^2(p_x^2+p_y^2)\}}\cdot T - p_x x - p_y y \quad , \tag{6}$$

and

$$Q(p_x,p_y) = \begin{vmatrix} \partial^2\phi/\partial p_x^2 & \partial^2\phi/\partial p_x\partial p_y \\ \partial^2\phi/\partial p_x\partial p_y & \partial^2\phi/\partial p_y^2 \end{vmatrix} \quad . \tag{7}$$

The main contribution of the integral in eq. (4) comes from the point $(p_x^0,p_y^0)$ where the phase of the integrand is stationary, i.e., where

$$\begin{aligned} \partial\phi(p_x,p_y)/\partial p_x &= -[V_{rms}^2 p_x t/\sqrt{\{1 - V_{rms}^2(p_x^2+p_y^2)\}}] + x = 0 \\ \partial\phi(p_x,p_y)/\partial p_y &= -[V_{rms}^2 p_y t/\sqrt{\{1 - V_{rms}^2(p_x^2+p_y^2)\}}] + y = 0 \end{aligned} \quad . \tag{8}$$

Substituting the $p_x^0$ and $p_y^0$ into eq. (5), we can obtain the travel time and amplitude of seismic wave

$$\tau = \phi(p_x^0,p_y^0) \quad , \tag{9}$$

and

$$A = \omega/2\pi|Q(p_x^0,p_y^0)|^{1/2} \quad . \tag{10}$$

Assuming that there is a spiky wavelet at the source position, the imaging of a seismic trace can be expressed as

$$I(x,y,T) = (A_g/A_s) \int f(\omega)\omega\exp(-j\pi/2)\exp[-j\omega(t_s + t_g)]d\omega$$

$$= (A_g/A_s)F'(t_s + t_g) \quad , \tag{11}$$

where $F'(t)$ is the first-order time derivative of a trace, $A_s$ and $t_s$ are amplitude and traveltime of wavefield from source position $(x_s,y_s,0)$ to imaging position $(x,y,T)$, $A_g$ and $t_g$ are amplitude and traveltime of wavefield from geophone position $(x_g,y_g,0)$. Eq. (11) shows that the migration of a trace can be performed by picking the value at $(t_s + t_g)$ sample of the first-order time derivative of the trace.

Based on geometry, we can get the incident angle, defined as the half of the angle between incident wave and reflected wave,

$$\theta = \tfrac{1}{2} \arccos[(\tau_{SI}^2 V_{rms}^2 + \tau_{GI}^2 V_{rms}^2 + r_{SG}^2)/(2\tau_{GI}\tau_{SI}V_{rms}^2)] \quad , \tag{12}$$

where $\tau_{SI}$ and $\tau_{GI}$ are the traveltime from the source position and the geophone position to the imaging position, respectively, $r_{SG} = \sqrt{\{(x_s-x_g)^2 + (y_s-y_g)^2\}}$. is the length of the source position to the geophone position (offset), $V_{rms}$ is the root-mean-square velocity of imaging point. Then we stack the values of imaged gathers into different angle bins according to eq. (12) to extract angle gathers.

## Estimation of Fresnel Zone

Since the specular reflections and diffractions can be separated based on the angles, we remove the reflections by muting the Fresnel zones of reflections, i.e., the neighborhoods of apices of concave shapes related to the reflections on angle gathers. An accurate estimation of the Fresnel zone then becomes crucial because little residual reflection energy will mask the diffraction images. We evaluate the Fresnel zones under tilted reflector by following the analytical derivation of pre-stack time migration.

Fig. 1 illustrates the estimation of Fresnel zone at imaging point I for a tilted reflector AB under the root-mean-square velocity is $V_{rms}$. We assume that the limit of constructive interference zone (Fresnel zone) is related to the migrated event at point P in the angle gather. Based on the wave theory, the distance between I and P is supposed as $\delta = 1/(2Tf_d)$, where $f_d$ is the dominant frequency of recorded data. Based on the migration theory, the migrated event at point P is considered as the reflection resulting from point Q on reflector AB for the incident wave from shot S. We construct the two equations about traveltime and incident/reflected angle using the geometry method that reads

$$\sqrt{\{(TV_{rms} - d\sin\alpha)^2 + (x + d\cos\alpha - x_s)^2\}}$$

$$+ \sqrt{\{(TV_{rms} - d\sin\alpha)^2 + (x + d\cos\alpha - x_r)^2\}}$$

$$= \sqrt{\{V_{rms}^2[T - 1/(2f_d)]^2 + (x - x_s)^2\}}$$

$$+ \sqrt{\{V_{rms}^2[T - 1/(2f_d)]^2 + (x - x_r)^2\}} \quad , \tag{13a}$$

$$[\sin\alpha(x + d\cos\alpha - x_s) + \cos\alpha(TV_{rms} - d\sin\alpha)]$$

$$/\sqrt{\{(x + d\cos\alpha - x_s)^2 + (TV_{rms} - d\sin\alpha)^2\}}$$

$$= [\sin\alpha(x + d\cos\alpha - x_r) + \cos\alpha(TV_{rms} - d\sin\alpha)]$$

$$/\sqrt{\{(x + d\cos\alpha - x_r)^2 + (TV_{rms} - d\sin\alpha)^2\}} \quad , \tag{13b}$$

where we introduce an intermediate variable d that denotes the distance between point I and Q along the reflector; $x_r$ and $x_s$ are the lateral coordinates of receiver R and shot S, respectively, (x,T) is the lateral coordinate and traveltime of point I, $T-1/(2f_d)$ is the traveltime of point P, $(x + d\cos\alpha, T - d\sin\alpha/V_{rms})$ is the lateral coordinate and traveltime of point Q,$(\cos\alpha,\sin\alpha)$ is the direction cosines of the normals to the reflector. We will solve $x_r$ and d under given $x_s$ and (x,T) from eq. (13) and the assumption that the variations of $V_{rms}$ among points I, Q, and P can be neglected.

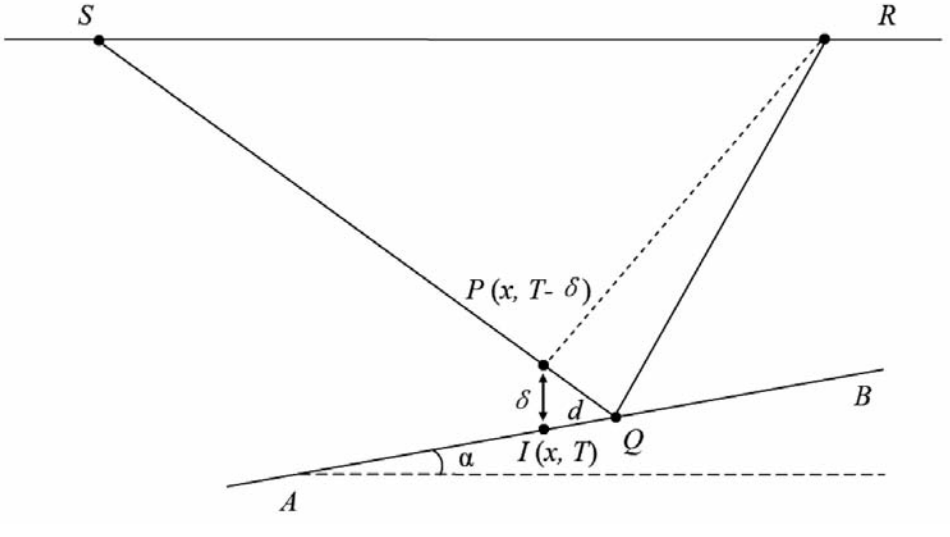


Fig. 1. Illustration of the estimation of the Fresnel zone. Line segment AB denotes a tilted reflector. Points S and R denote shot and receiver, respectively. Points I and Q are two neighboring points on the reflector with a distance of d. Reflector AB has a dip angle of $\alpha$. The migrated event at point P is considered as the reflection resulting from point Q.

Due to the fact that $\varepsilon = d/TV_{rms}$ and $\delta$ are two non-dimensional small numbers in discussion, we approximately solve eq. (13) by neglecting $\varepsilon$- and $\delta$-related higher-order terms. Firstly, we define angles $\varphi$, $\phi$. and related small angles $\Delta\varphi$, $\Delta\phi$, that read

$$\sin\varphi = (x - x_s)/\sqrt{\{(x - x_s)^2 + T^2V_{rms}^2\}} \quad , \tag{14}$$

$$\sin(\varphi+\Delta\varphi) = (x + d\cos\alpha - x_s)/\sqrt{\{(x + d\cos\alpha - x_s)^2 + T^2V_{rms}^2\}}$$

$$\approx \sin\varphi - \Delta\varphi\cos\varphi \quad , \tag{15}$$

$$\sin\phi = (x + d\cos\alpha - x_r)/\sqrt{\{(x + d\cos\alpha - x_r)^2 + T^2V_{rms}^2\}} \quad , \tag{16}$$

$$\sin(\phi+\Delta\phi) = (x - x_r)/\sqrt{\{(x - x_r)^2 + T^2V_{rms}^2\}}$$

$$\approx \sin\phi - \Delta\varphi\cos\phi \quad . \tag{17}$$

From eqs. (14), (15), (16) and (17) we have

$$\Delta\varphi \approx \varepsilon\cos\varphi\cos(\alpha-\varphi) \quad , \tag{18}$$

$$\Delta\phi \approx -\varepsilon\cos\phi\cos(\alpha-\phi) \quad . \tag{19}$$

Substituting eqs. (14)-(19) into eqs. (13a) and (13b) and neglecting $\delta$-, $\Delta\varphi$- and $\Delta\phi$-related higher-order terms yields

$$[\cos^2(\alpha-\varphi)/\cos\varphi]\varepsilon^2 - 2[(\sin\alpha/\cos\varphi)-\tan\varphi\cos(\alpha-\varphi)]\varepsilon - 2\delta\cos\varphi = 0 \quad . \tag{20}$$

Two roots $\varepsilon^{\pm}$ can be obtained from eq. (20) and be substituted into equations $d^2 = TV_{rms}\varepsilon^{\pm}$. Then substituting the resulting values into eqs. (16) and (13), we can obtain the two solutions of $x_g$. Here, the two solutions are related to the lower and upper limits of the Fresnel zone. The lower and upper angles corresponding to the lower and upper limits of the Fresnel zone are then obtained by substituting the resulting values into eq. (12).

Unfortunately, the structural dip $\alpha$ in the above equations, which play pivotal roles in attenuating reflections, is unknown. Thus, we present a structural dip field estimation method by scanning. We mute the Fresnel zone by a group of changing parameters $\alpha$, and then pick the structural dips which can remove the corresponding reflected events completely.

This method results in attenuating both specular and diffracted wave components. However, the specular component is attenuated more than the diffracted component. This is because the data subject to migration, nearly all the specular energy is concentrated within the respective Fresnel zones on

imaging hyperbolae, while the diffracted events extend straight and will be enhanced in the stacking processing. This technique has proven to be a useful tool in solving the problem of imaging diffractions masked by strong specular reflections.

## Demigration and remigration of the diffraction field

In fact, we can obtain pre-stack time diffraction migration sections mentioned by the scheme mentioned above. Since the pre-stack time migration method cannot effectively handle strong velocity heterogeneities, we introduce a demigration method to remove the previous migration effect and to obtain the diffracted wavefield. For an imaging section $S_I$ resulted from a shot gather, we first calculate the travel time $\tau_1$ and amplitude weight $A_1$ of the wavefield from the source position to the imaging position, and the travel time $\tau_2$ and amplitude weight $A_2$ of the wavefield from the imaging position to the geophone position by eqs. (9) and (10). After preparing a new array D for the diffracted wavefield, we obtain the diffracted wavefield

$$D(x_D,y_D,t_D) = \sum_{\tau_1+\tau_2=t_D} S_I(x_1,y_1,T_1)A_1A_2 \quad , \tag{21}$$

where $D(x_D,y_D,t_D)$ is the value at $t_D$ in the diffracted wavefield locating geophone at $(x_D,y_D)$, $S_I(x_1,y_1,T_1)$ is the value at $T_1$ in the stacked diffraction migration section located at $(x_1,y_1)$ and satisfy the condition of $\tau_1 + \tau_2 = t_D$. Since the calculations of traveltime are reciprocal in the processes of migration and demigration, even if $V_{rms}$ is not perfect for complex geological structure, it will not affect the practical application of my method. Because the diffraction imaging is used to detect and map the positions of small scale geological discontinuities, the amplitude errors caused in the processes of migration and demigration are acceptable too.

Taking computation efficiency into consideration, we choose wave equation migration instead of reverse time migration to image the diffracted wavefield to map the positions of small scale geological discontinuities. In this paper, we use the optimum split-step Fourier wave equation migration method (Liu and Zhang, 2006; Zhang and Liu, 2007) to perform the depth migration.

## NUMERICAL IMPLEMENTATIONS

A 2D numerical model, as shown in Fig. 2, was created to evaluate the effectiveness of my workflows. The model includes three dipped thin layers with small-scale faults, two curved interfaces with small-scale velocity discontinuities

along the interfaces, and one pinch-out. The 10-meter-size velocity discontinuities and 2.5-meter-size faults are indicated by the rectangles and the squares in Fig. 2, respectively. The synthetic data set was generated using a 25-Hz Ricker wavelet and a 2-ms-time-sampling interval.

To avoid the artifacts caused by the staircase approximation to the curved interface and dipped thin layers in the finite-difference data modeling, an irregular and unstructured-grid method modeling scheme (Zhang and Liu, 1999) was used to model the shot gathers. A shot record (Fig. 3) shows that the diffractions from the small-scale velocity discontinuities are indeed completely concealed by the strong reflected events.

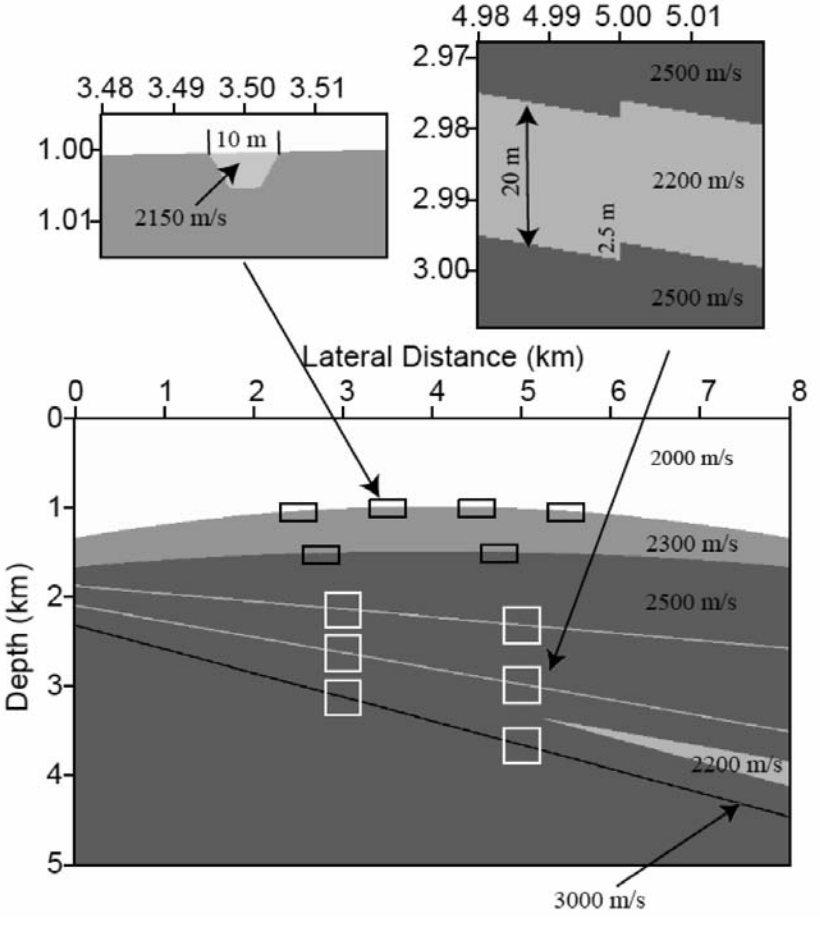


Fig. 2. Subsurface velocity model used to generate the synthetic data set. The model includes six small-scale faults indicated by the squares, six small velocity discontinuities indicated by the rectangles, and one pinch-out. The upper-right and -left small figures are the enlarged details around a typical fault and a typical velocity discontinuity, respectively. The exact velocities and sizes are printed in the figures.

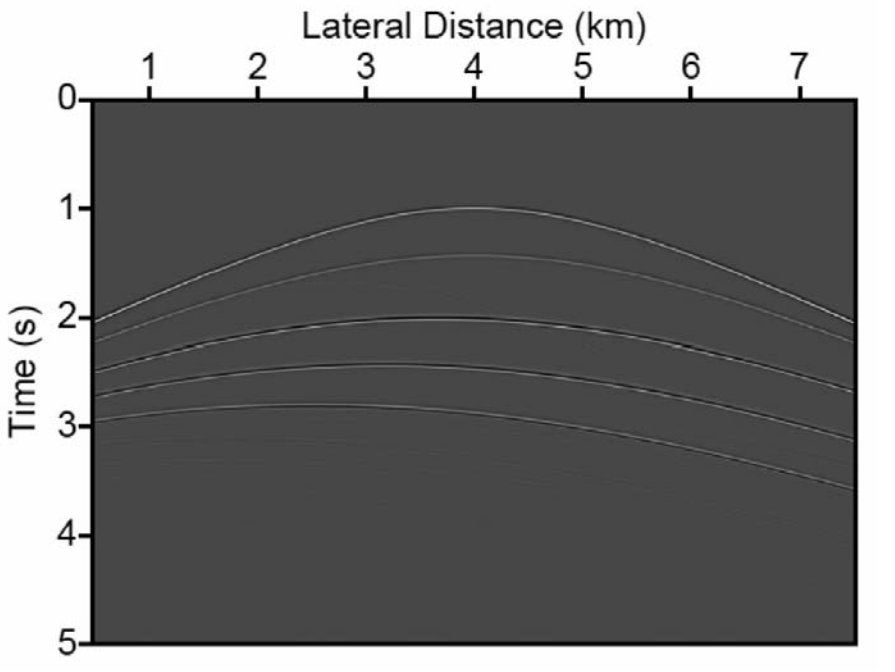


Fig. 3. A typical shot gather for the shot positioned at the lateral distance of 4 km and obtained by the grid method modeling scheme. We see the great amplitude differences between specular reflections and diffractions.

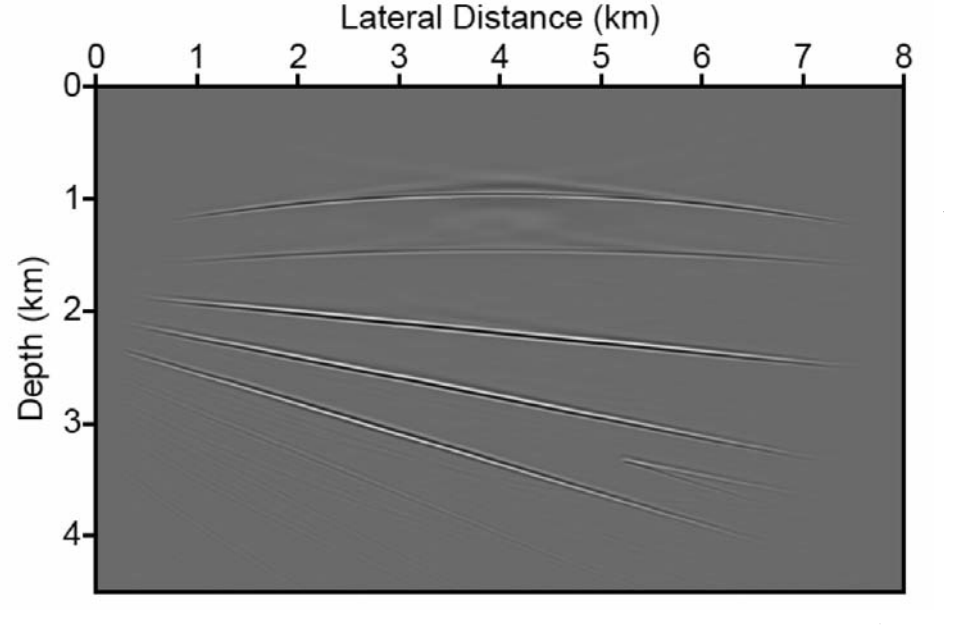


Fig. 4. Migration stacked section from the original reflection shot records by wave equation migration. We see clearly the dipped thin layers, curved interfaces, and pinch-out but no faults and velocity discontinuities.

Fig. 4 shows the migration stacked section by pre-stack wave-equation migration from the original reflection shot records. We see clearly the dipped thin layers, curved interfaces, and pinch-out body but cannot identify the faults and velocity discontinuities. Since we do not know the structural dip in practical case, we extract dip scanning gathers by muting the Fresnel zone of reflections using a group of changing structural dip, shown as in Fig. 5. The solid line denotes the picked structural dip which can remove the corresponding reflected events completely. Fig. 6 show the comparison between the authentic dip field (Fig. 6a) and the structural dip field estimated by my method (Fig. 6b). The errors in the left and right side of the field are caused by the obscure imaging. Fig. 7a shows an angle gather at the lateral distance of 3 km corresponding to the shot gather of Fig. 3, while Fig. 7b shows the angle gather after muting using the resulting Fresnel zone. We see the neighborhoods of apices related to the reflections are removed.

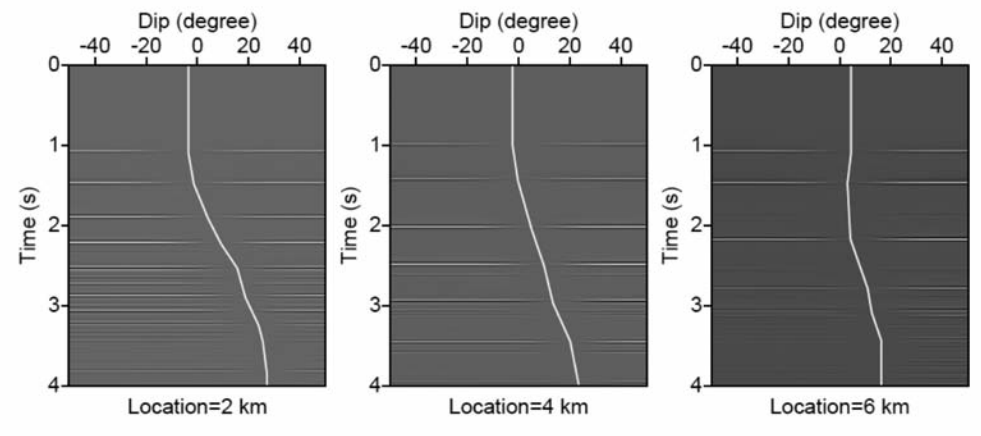


Fig. 5. Dip scanning gathers positioned at the lateral distance of 2 km, 4 km and 6 km, which are extracted by muting the Fresnel zone of reflections using a group of changing structural dip. The solid line denotes the picked structural dip which can remove the corresponding reflected events completely.

Fig. 8 shows the diffraction imaging section from a shot record by pre-stack time diffraction migration. The diffracted wavefield, shown as in Fig. 9, is obtained by demigration from the diffraction imaging section (Fig. 8). Contrasting with the original shot gather shown in Fig. 3, the diffracted component is enhanced while the reflected component is attenuated completely. The final diffraction migration section (Fig. 10), obtained by my method shows that the small size faults and velocity discontinuities, are clearly imaged and can be easily interpreted.

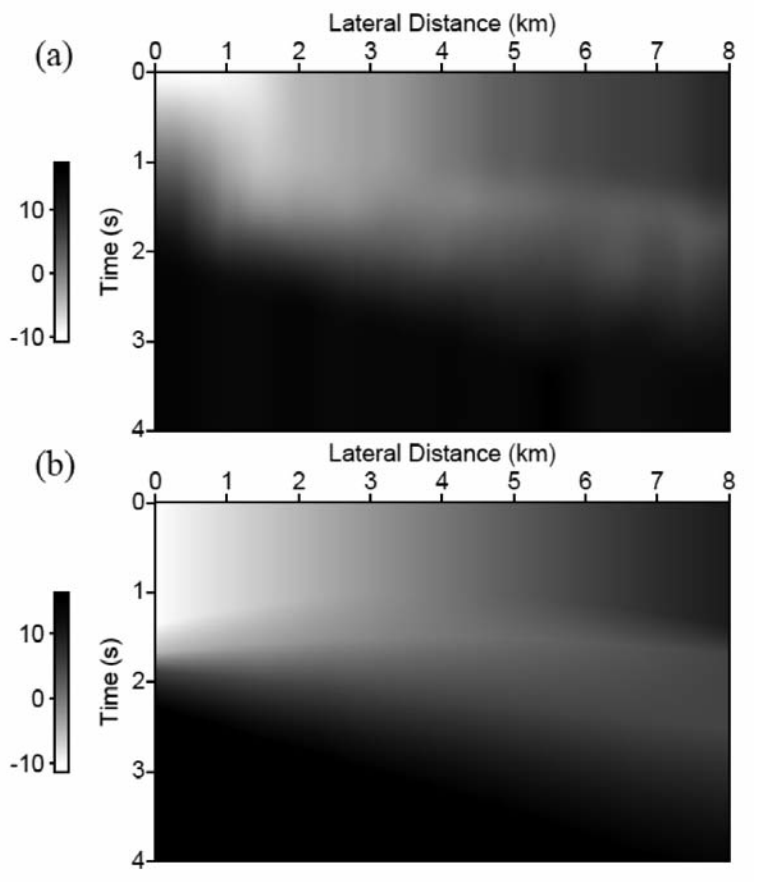


Fig. 6. Comparison between the authentic dip field (a) and the dip field estimated by my method (b). The errors in the left and right side of the field are caused by the obscure imaging.

We further test my methodology on a field data example. Fig. 11 shows the migration stacked section obtained using pre-stack wave equation migration from original reflected wavefield data set. Fig. 12 shows the diffraction images obtained using my method from diffracted wavefield. Note that continuous reflection events, as shown in Fig. 11, have been removed. In order to remove the reflections completely for deep complex structure, we have to over mute the reflections (increase the $\delta$), which led to low amplitude for the shallow part of the section. The diffraction images of Fig. 12 will contribute to the interpretation of conventional migration section (e.g., Fig. 11) in detecting small-scale faults and heterogeneities. Fig. 13 compares the enlarged details around a small window in Figs. 11 and 12. We see certain fractures and uncertain faults in the migration section of conventional reflection migration (Fig. 13a) and clear diffraction images at the corresponding locations in the migration section of diffraction migration (Fig. 13b).

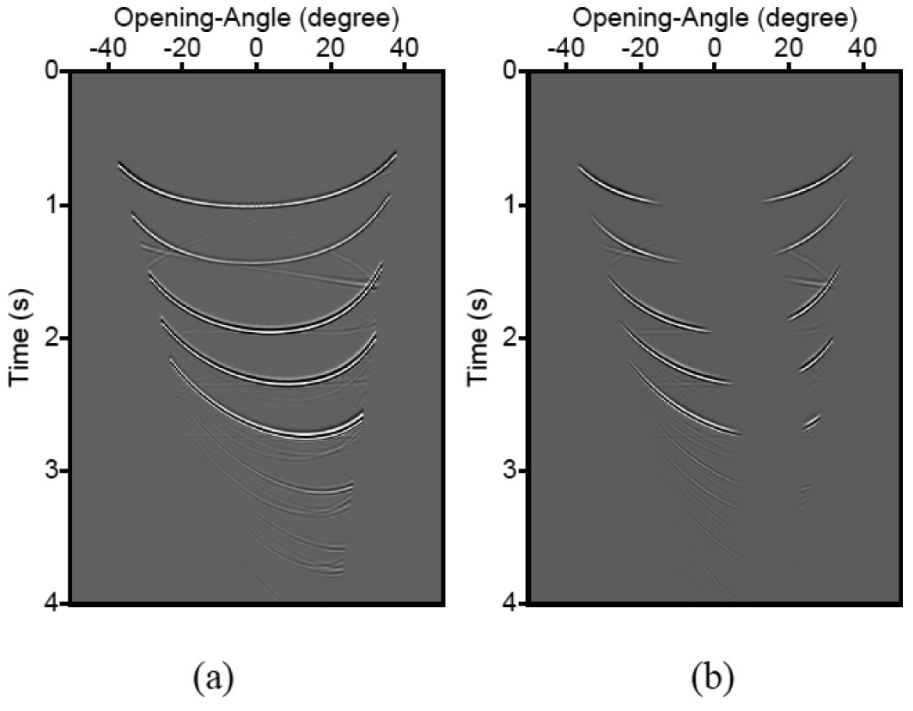


Fig. 7. The angle gather (a) at the lateral distance of 3 km corresponding to the shot gather of Fig. 3 and the same angle gather after muting (b). We see the neighborhoods of apices related to the reflections are removed.

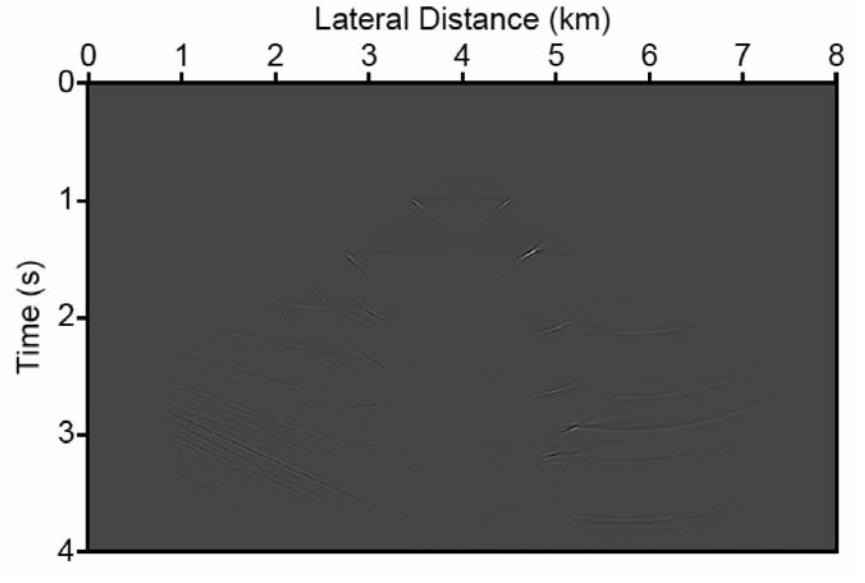


Fig. 8. The shot-domain diffraction wave imaging section resulted from a shot record (Fig. 3) by pre-stack time diffraction migration.

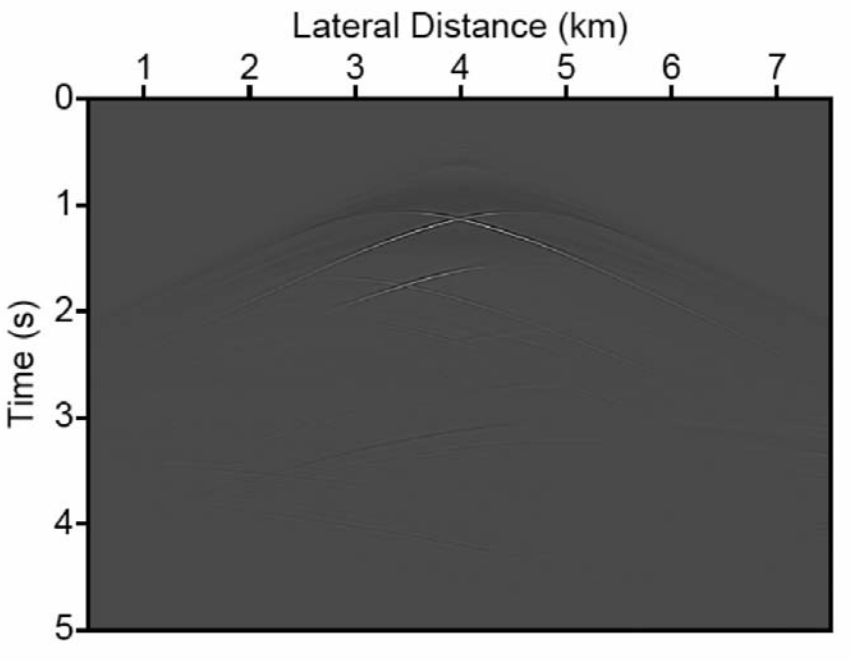


Fig. 9. The diffracted wavefield resulting from the shot-domain diffraction imaging section (Fig. 8) by demigration from the diffraction imaging section (Fig. 8). Contrasting with the original shot gather shown in the Fig. 3, the diffracted component is enhanced while the reflected component is attenuated completely.

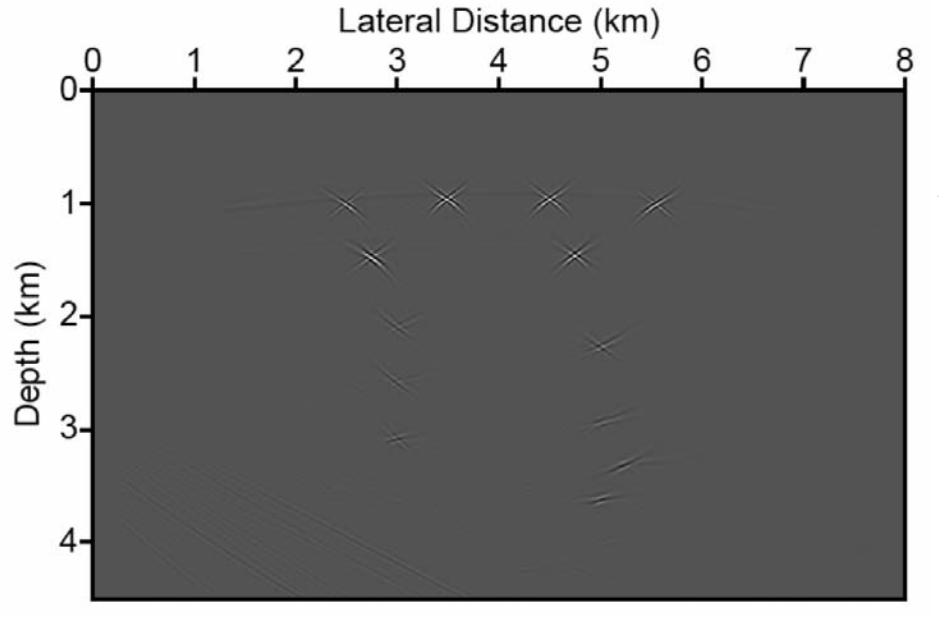


Fig. 10. The diffraction migration section resulting by my workflow. We see that the faults, velocity discontinuities as well as pinch-out, as shown in Fig. 2, are correctly imaged.

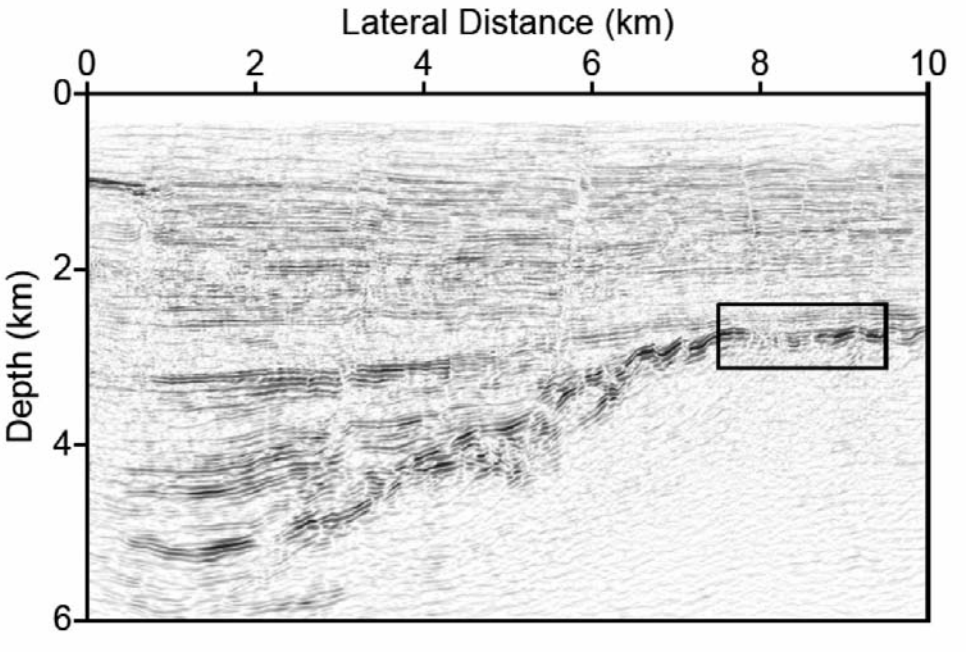


Fig. 11. Migration stacked section obtained using pre-stack wave equation migration from original reflected wavefield data set.

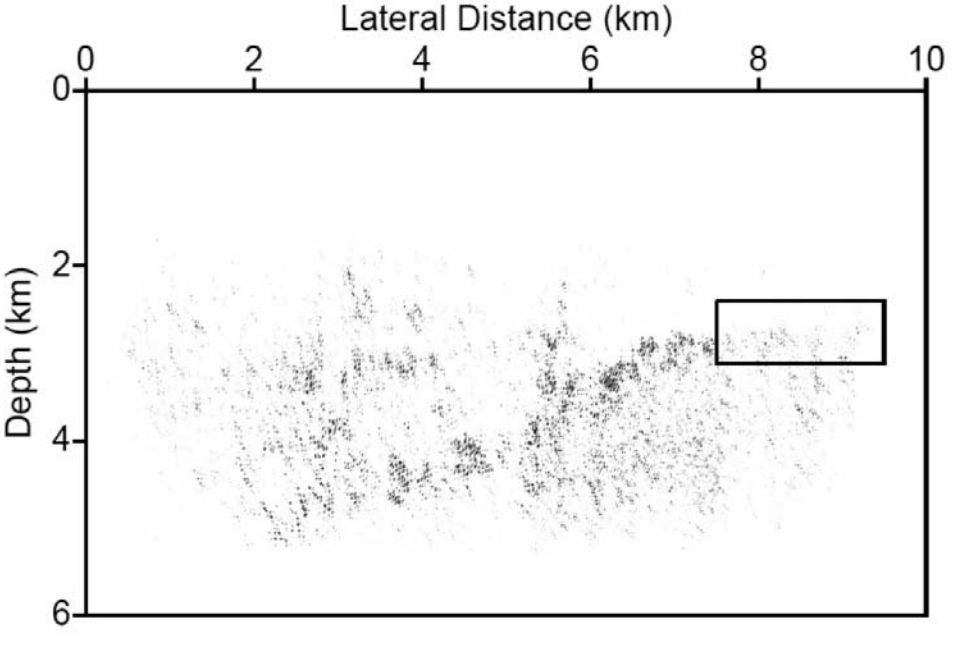


Fig. 12. Migration stacked section obtained using my method from diffracted wavefield. Note that continuous reflection events, as shown in Fig. 11, have been removed.

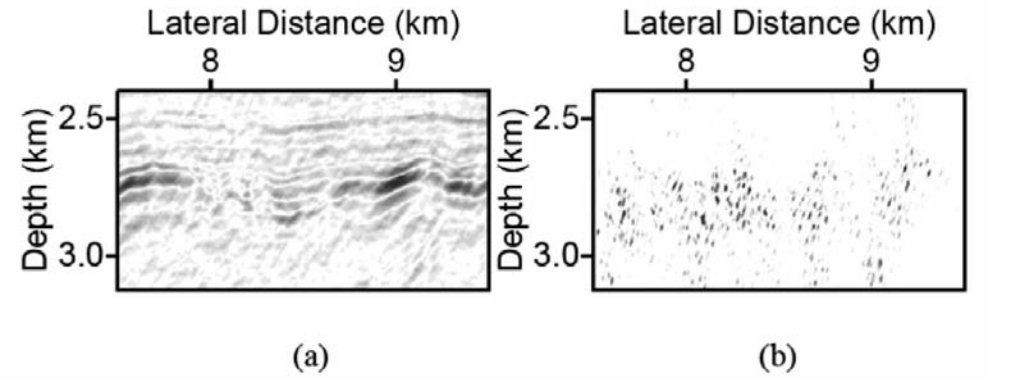


Fig. 13. Comparison between the migration results obtained reflected wavefield (a) and diffracted wave field (b). The display is the enlarged details around a small window in Figs. 11 and 12. We see certain fractures and uncertain faults in Fig. 13a and corresponding diffraction images in Fig. 13b.

## CONCLUSIONS

We demonstrate a robust workflow to remove specular reflections and image the diffractions. This imaging algorithm provides a super-resolution in detecting small-scale faults and velocity heterogeneities in the seismic imaging. The result of my method is an effective complement to conventional interpretation workflow. Numerical and field data examples demonstrate that my method is capable of properly imaging diffracted energy and revealing important structural elements, even the details smaller than the seismic wavelength, which may be concealed otherwise in the conventional seismic processing. We believe that such images should be made available to the interpreter as a supplement to reflected wavefield seismic images.

## ACKNOWLEDGEMENTS

Thanks to the National Natural Science Fund of China (under grant 41174112), the National Major Project of China (under grant 2011ZX05008-006 and 2011ZX05023-005) who supported this work.

## REFERENCES

Bansal, R. and Imhof, M.G., 2005. Diffraction enhancement in prestack seismic data. Geophysics, 70: V73-V79.

Bertero, M., Boccacci, P. and Piana, M., 1997. Resolution and Super-resolution in Inverse Diffraction. Proc. Conf. Inverse Problems of Wave Propag. Diffrac.: 1-17, Springer Verlag, Berlin.

Bleistein, N., 1984. Mathematical Methods for Wave Phenomena. Academic Press, Inc., New York.

Docherty, P., 1991., A brief comparison of some Kirchhoff integral formulas for migration and inversion. Geophysics, 56: 1164-1169.

Gazdag, J., 1978. Wave-equation migration with the phase shift method. Geophysics, 43: 1342-1351.

Claerbout, J.F., 1985. Imaging the Earth's Interior. Blackwell Scientific Publications, Oxford.

Cheng, M. and Hilterman, F., 2007. Scattering object imaging with azimuthal binning to detect vertical fractures. Expanded Abstr., 77th Ann. Internat. SEG Mtg., San Antonio: 2045-2049.

Goldin, S., Khaidukov, V., Kostin, V., Ryan, S. and Tcheverda, V., 2000. Separation of reflected and diffracted objects by means of Gaussian beams decomposition. In: Bermudez, A., Gomez, D., Hazard, C., Joly, P. and Roberts, J. (Eds.), Proc. 5th Internat. Conf. Mathemat. Numer. Asp. Wave Propag.: SIAM-INRIA.

Khaidukov, V., Landa, E. and Moser, T.J., 2004. Diffraction imaging by focusing-defocusing. An outlook on seismic superresolution. Geophysics, 69: 1478-1490.

Kovalevsky, G.L., 1971. Kinematic and some dynamic features of diffracted seismic waves. Geol. Geophys., 7: 101-110 (in Russian).

Landa, E. and Maximov, A., 1980. Testing of algorithm for low-amplitude fault detection. Geol. Geophys., 12: 108-113 (in Russian).

Liu, L. and Zhang, J., 2006. 3D wavefield extrapolation with optimum split-step Fourier method. Geophysics, 71: 95-108.

Moser, T. and Howard, C.B., 2008. Diffraction imaging in depth. Geophys. Prosp., 56: 627-641.

Reshef, M. and Landa, E., 2009. Post-stack velocity analysis in the dip-angle domain using diffractions. Geophys. Prosp., 57: 811-823.

Sava, P., Biondi, B. and Etgen, J., 2005. Wave-equation migration velocity analysis by focusing diffractions and reflections. Geophysics, 70: U19-U27.

Taner, M.T., Fomel, S. and Landa, E., 2006. Prestack separation of seismic diffractions using planewave decomposition. Expanded Abstr., 76th Ann. Internat. SEG Mtg.,New Orleans: 2401-2404.

Verschuur, D., Wang, D. and Hermann, F., 2007. Multi-term multiple prediction using separated reflections and diffractions combined with curvelet-based subtraction. Expanded Abstr., 77th Ann. Internat. SEG Mtg., San Antonio: 2535-2539.

Zhang, J. and Liu, L., 2007. Optimum split-step Fourier 3D depth migration: Developments and practical aspects. Geophysics, 72: 167-175.

Zhang, J. and Liu, T., 1999. P-SV-wave propagation in heterogeneous media: grid method. Geophys. J. Internat., 136: 431-438.

Zhang, J., Xu, J. and Zhang, H., 2012. Migration from 3D irregular surfaces: A prestack time migration approach. Geophysics, 77: S117-S129.

Zhu, X. and Wu, R., 2008. Imaging diffraction points using the local image matrix in prestack migration. Expanded Abstr., 78th Ann. Internat. SEG Mtg., Las Vegas: 2161-2165.

Zhu, X. and Wu, R. 2010. Imaging diffraction points using the local image matrix generated in prestack migration. Geophysics, 75: S1-S9.